7-5-2018

What Powered the Optical Transient AT2017gfo Associated with GW170817?

Shao-Ze Li
Central China Normal University; University of Nevada, Las Vegas

Liang-Duan Liu
University of Nevada, Las Vegas; Nanjing University; Key Laboratory of Modern Astronomy and Astrophysics (Nanjing University), Ministry of Education

Yun-Wei Yu
Central China Normal University; Key Laboratory of Quark and Lepton Physics (Central China Normal University), Ministry of Education

Bing Zhang
University of Nevada, Las Vegas, bing.zhang@unlv.edu

Repository Citation
Li, S., Liu, L., Yu, Y., Zhang, B. (2018). What Powered the Optical Transient AT2017gfo Associated with GW170817?. *Astrophysical Journal, 861*(2), 1-7.
http://dx.doi.org/10.3847/2041-8213/aace61

The Astrophysical Journal Letters, 861:L12 (7pp), 2018 July 10 https://doi.org/10.3847/2041-8213/aace61

What Powered the Optical Transient AT2017gfo Associated with GW170817?

Shao-Ze Li[1,2], Liang-Duan Liu[2,3,5], Yun-Wei Yu[1,4], and Bing Zhang[2]
[1] Institute of Astrophysics, Central China Normal University, Wuhan 430079, People's Republic of China; yuyw@mail.ccnu.edu.cn
[2] Department of Physics and Astronomy, University of Nevada Las Vegas, Las Vegas, NV 89154, USA; zhang@physics.unlv.edu
[3] School of Astronomy and Space Science, Nanjing University, Nanjing 210093, People's Republic of China
[4] Key Laboratory of Quark and Lepton Physics (Central China Normal University), Ministry of Education, Wuhan 430079, People's Republic of China
[5] Key Laboratory of Modern Astronomy and Astrophysics (Nanjing University), Ministry of Education, Nanjing 210093, People's Republic of China
Received 2018 April 18; revised 2018 June 11; accepted 2018 June 19; published 2018 July 5

Abstract

The groundbreaking discovery of the optical transient AT2017gfo associated with GW170817 opens a unique opportunity to study the physics of double neutron star (NS) mergers. We argue that the standard interpretation of AT2017gfo as being powered by radioactive decay of *r*-process elements faces the challenge of simultaneously accounting for the peak luminosity and peak time of the event, as it is not easy to achieve the required high mass, and especially the low opacity of the ejecta required to fit the data. A plausible solution would be to invoke an additional energy source, which is probably provided by the merger product. We consider energy injection from two types of the merger products: (1) a post-merger black hole powered by fallback accretion; and (2) a long-lived NS remnant. The former case can only account for the early emission of AT2017gfo, with the late emission still powered by radioactive decay. In the latter case, both early- and late-emission components can be well interpreted as due to energy injection from a spinning-down NS, with the required mass and opacity of the ejecta components well consistent with known numerical simulation results. We suggest that there is a strong indication that the merger product of GW170817 is a long-lived (supramassive or even permanently stable), low magnetic field NS. The result provides a stringent constraint on the equations of state of NSs.

Key words: accretion, accretion disks – gravitational waves – stars: black holes – stars: neutron

1. Introduction

The discovery of the first gravitational wave (GW) event, i.e., GW150914 from a merger of double black holes (BHs), marked the beginning of the era of GW astronomy (Abbott et al. 2016). On 2017 August 17, the Laser Interferometer Gravitational-Wave Observatory (LIGO)/Virgo detector network further detected a historical event GW170817, the first GW event from the merger of a neutron star–neutron star (NS–NS) binary (Abbott et al. 2017a), which was followed by a short-duration gamma-ray burst (GRB) dubbed GRB 170817A, captured by the Fermi satellite 1.7 s after the GW merger event (Goldstein et al. 2017; Savchenko et al. 2017; Zhang et al. 2018). The GW170817/GRB 170817A association robustly confirmed the long-standing hypothesis that short GRBs originate from compact star mergers involving at least one NS. The apparently low radiation luminosity and energy of GRB 170817A are consistent with having this GRB being observed at a large viewing angle from the jet axis (Abbott et al. 2017b), which causes the missing afterglow emission during the first ∼10 days in follow-up observations (Troja et al. 2017). Nevertheless, during this period, a significant ultraviolet–optical–infrared (UVOIR) transient was detected, first announced by Coulter et al. (2017) and subsequently observed by many groups (e.g., Arcavi et al. 2017; Lipunov et al. 2017; Tanvir et al. 2017; Valenti et al. 2017). This transient, named as AT2017gfo/SSS17a/DLT17ck (hereafter AT2017gfo), was thought to be associated with an NS–NS merger (Li & Paczyński 1998) that has been called a "kilonova" (Metzger et al. 2010) or a "mergernova" (Yu et al. 2013; Li & Yu 2016). In this Letter, we use the term "mergernova" for the following two reasons: (1) a "kilonova" is defined as being powered by radioactive decay. As shown below, we invoke energy injection from a central engine to account for the observations. The term "mergernova" broadly defines the merger-associated UVOIR transients, regardless of the energy power. (2) The reason for adopting the kilonova terminology was that the peak luminosity is about 1000 times of that of a typical nova, which is 10^{41} erg s^{-1}. The earliest observational data point of AT2017gfo already has a luminosity above 10^{42} erg s^{-1}, at least one order of magnitude brighter than the typical luminosity of kilonovae. As shown by Yu et al. (2013) and Metzger & Piro (2014), the existence of a long-lived NS as the post-merger product can increase the peak luminosity significantly. A BH central engine with additional accretion activities may also act as a source of energy injection to the mergernova (Ma et al. 2018; Song et al. 2018).

The property of a radioactivity-powered mergernova primarily depends on the mass and the opacity of the ejecta. In particular, the existence of lanthanides, even with a small mass fraction (e.g., $\sim 10^{-4}$), would increase the Planck mean opacity by as much as $\sim$(10–100) cm^2 g^{-1} (Kasen et al. 2013), so that the peak time of the event will be shifted to about one week after the merger, with a redder spectrum at the peak (Barnes & Kasen 2013; Tanaka & Hotokezaka 2013). In any case, a polar outflow, most likely launched by a disk wind and irradiated by neutrino emission, may still give rise to an early "blue" component because lanthanide synthesis is probably inefficient there (Metzger & Fernández 2014). The observed AT2017gfo emission can be indeed understood with such a "blue+red" radioactivity-powered mergernova model (e.g., Cowperthwaite et al. 2017; Nicholl et al. 2017; Smartt et al. 2017; Tanaka et al. 2017; Villar et al. 2017).[6] Specifically, the interpretation of the peak luminosity $\sim 10^{42}$ erg s^{-1} and the peak time ∼1 day in this model requires a relatively low

[6] In some papers, the dynamical ejecta is interpreted as "blue", whereas the disk wind outflow as "red" (e.g., Kasen et al. 2017).

opacity ($\kappa \sim 0.3\,\mathrm{cm^2\,g^{-1}}$), a relatively large ejecta mass ($M \sim 0.04\,M_\odot$), and a relatively high characteristic velocity ($v \sim 0.3c$) for the blue component. These requirements push the boundary of numerical simulations regarding the ejected mass (Dessart et al. 2009; Fernández & Metzger 2013; Perego et al. 2014; Just et al. 2015; Richers et al. 2015; Shibata et al. 2017) and the expected opacity, which is believed to be, at least, not much lower than $\sim 1\,\mathrm{cm^2\,g^{-1}}$ (Kasen et al. 2013; Tanaka et al. 2018).

Metzger et al. (2018) argued that a short-lived hypermassive NS with a surface magnetic field of $B \sim 10^{14}$ G could help to increase the mass of a disk wind. Radice et al. (2018) also suggested that the viscous ejecta can be as much as $0.1\,M_\odot$. These can partially decrease the difficulty of the radioactive mergernova model, but the required low opacity may not be readily accounted for. Alternatively, if the remnant NS is long-lived, then the mergernova emission itself would be significantly affected by the NS due to the additional energy injection from the NS and the effect of ionization (Yu et al. 2013; Metzger & Piro 2014). Recently, Yu et al. (2018) showed that the observed emission from AT2017gfo can be accounted for by a hybrid model, with the early emission powered by radioactivity and later emission powered by energy injection from a long-lived, low-field pulsar.[7] In their modeling, all of the emission comes from the same ejecta component, with a single uniform opacity around $1\,\mathrm{cm^2\,g^{-1}}$ and a total mass of $\sim 0.03\,M_\odot$. The latter is less than half of the total mass invoked to interpret the event using the radioactive heating alone (e.g., $0.065\,M_\odot$; Villar et al. 2017). It remains unclear whether ionization by the pulsar wind can penetrate deep enough to reduce the opacity of the entire ejecta to around $\sim 1\,\mathrm{cm^2\,g^{-1}}$.

This Letter includes two parts. The first part (Section 2) presents an argument against the traditional radioactivity-powered mergernova model; specifically, the difficulty in simultaneously accounting for both the high luminosity (high mass) and early peak time (low opacity). Encouraged by Yu et al. (2018), the second part (Section 3) presents our modeling of AT2017gfo within the framework of engine-powered mergernova. We show that without an ad hoc mechanism to drastically reduce the opacity of the merger ejecta and with a reasonable amount of ejecta mass (a few $10^{-3}\,M_\odot$), the observational data can be accounted for, given that the merger left behind a long-lived, low-B NS.

2. The Radioactivity Power

In the traditional radioactivity-powered mergernova (kilonova) model, the parameters of the blue-component ejecta (the polar disk wind) can be estimated from the peak of the observational bolometric light curve of AT2017gfo by the following analytical method. According to Arnett (1982), the peak bolometric luminosity is equal to the heating rate at the peak time, i.e.,

$$L_{\rm p} = \eta_{\rm th} M \varepsilon(t_{\rm p}), \tag{1}$$

where $\eta_{\rm th}$ is the thermalization efficiency, M is the ejecta mass, and ε is the heating rate per unit mass. The heating rate first remains constant for a duration of about one second and then

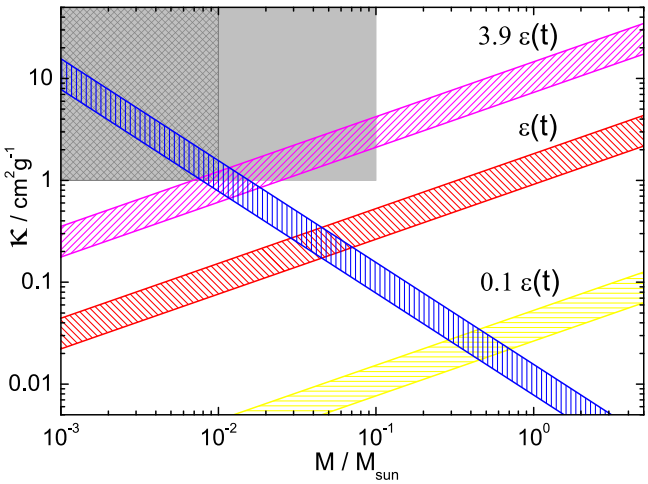

Figure 1. Constraints on the opacity κ and ejecta mass M for the blue component of AT2017gfo. The constraints from the peak time and peak luminosity are shown in the blue and red stripes, respectively, with the velocity constrained to $(0.3 \pm 0.1)c$. The preferred parameter regime based on numerical simulations and theoretical calculations is marked as gray area at the upper-left corner. The uniform+striped gray area and the striped gray area are for the dynamical ejecta and disk wind, respectively. Considering inefficient heating due to a large $Y_{\rm e}$ (favorable for a low κ) would reduce the heating rate by one order of magnitude (lower yellow stripe). Fixing $\kappa \sim 1\,\mathrm{cm^2\,g^{-1}}$, the required heating rate is larger than what radioactive heating can provide (upper magenta stripe), suggesting the existence of a central engine heating source.

decays following a power law that can be roughly estimated as Metzger et al. (2010), Korobkin et al. (2012)

$$\varepsilon(t) \approx 2 \times 10^{10}\,\mathrm{erg\,g^{-1}\,s^{-1}} \left(\frac{t}{1\,\mathrm{day}}\right)^{-\alpha}, \tag{2}$$

where $\alpha = 1.3$. One can further use the characteristic diffusion timescale of the ejecta to estimate the peak emission time, which reads (Metzger 2017)

$$t_{\rm p} = \left(\frac{3M\kappa}{4\pi\beta v c}\right)^{1/2} \approx 1.6\,\mathrm{days} \left(\frac{M}{0.01\,M_\odot}\right)^{1/2} \left(\frac{v}{0.1\,c}\right)^{-1/2} \left(\frac{\kappa}{1\,\mathrm{cm^2\,g^{-1}}}\right)^{1/2}, \tag{3}$$

where $\beta = 3$ is a dimensionless parameter characterized by the density profile of the ejecta. As a result, the peak luminosity can be determined to

$$L_{\rm p} = 1.2 \times 10^{41}\,\mathrm{erg\,s^{-1}} \times \left(\frac{M}{0.01\,M_\odot}\right)^{1-\alpha/2} \left(\frac{v}{0.1\,c}\right)^{\alpha/2} \left(\frac{\kappa}{1\,\mathrm{cm^2\,g^{-1}}}\right)^{-\alpha/2}, \tag{4}$$

where the thermalization efficiency is adopted as $\eta_{\rm th} \sim 0.5$ following Barnes et al. (2016). By taking the observational peak values of $L_{\rm p} \sim 10^{42}\,\mathrm{erg\,s^{-1}}$ and $t_{\rm p} \sim 1$ day, we can constrain M and κ from Equations (3) and (4) given a range of allowed ejecta velocity. The high $L_{\rm p}$ demands large M, large v, and small κ. In order to get a small $t_{\rm p}$, again a large v and small κ is preferred. We adopt a relatively large velocity $v \sim 0.3c$, but allow a range of $\pm 0.1c$ in our discussion. The required parameters are centered around $M \sim 0.04\,M_\odot$ and $\kappa \sim 0.3\,\mathrm{cm^2\,g^{-1}}$, as shown in Figure 1. Waxman et al. (2017)

[7] The relatively low luminosity of the prompt emission and broadband afterglow of GRB 170817A has also significantly constrained the properties of a putative underlying NS, with a dipolar magnetic field that should be significantly below the range of a typical magnetar (Ai et al. 2018; Geng et al. 2018).

also gave a constraint about the required opacity under the radioactivity-powered model, which should be at least $\lesssim 0.3\ \mathrm{cm^2\ g^{-1}}$. For comparison, we also present the allowed values of the parameters $M_{\rm ej}$ and κ in Figure 1, as shown by the gray area, where the upper limit on the ejecta mass is taken as $M < 0.1\,M_\odot$ for the dynamical ejecta (uniform+striped gray area) and $M < 0.01\,M_\odot$ for the disk wind (striped gray area; Bauswein et al. 2013; Hotokezaka et al. 2013; Rosswog 2013; Just et al. 2015; Richers et al. 2015; Shibata et al. 2017; Siegel & Metzger 2018). The lower limit on opacity is taken as $\kappa > 1\ \mathrm{cm^2\ g^{-1}}$ by considering the high velocity of the merger ejecta (Kasen et al. 2013; Tanaka et al. 2018). It is clearly shown that the required parameters by the radioactivity-powered mergernova model are far from the allowed parameter regions. This makes this model a disfavored one.

More specifically, although $M \sim 0.04\,M_\odot$ is already too high for a disk wind, it could still be acceptable if the merger product is a highly magnetized NS (Metzger et al. 2018). The more serious issue comes from the small opacity $\kappa \sim 0.3\ \mathrm{cm^2\ g^{-1}}$ demanded by the data. Detailed studies showed that the opacity depends on the electron fraction $Y_{\rm e}$, which defines how "neutron rich" the ejecta is. According to these studies, the *r*-process reactions are only efficient for an electron fraction of $Y_{\rm e} \lesssim 0.25$, in which case a remarkable number of heavy elements of a mass number $A > 130$ can be synthesized (Kasen et al. 2015; Rosswog et al. 2017). However, in the polar direction, the electron faction of a disk wind is probably higher than 0.25 due to the irradiation by the neutrino emission from the disk and, sometimes, from a remnant NS. Specifically, the electron fraction could be within the range of $Y_{\rm e} \sim 0.2$–0.4 if the remnant is a promptly formed BH (Fernández & Metzger 2013; Fernández et al. 2015) or $Y_{\rm e} \sim 0.3$–0.5 if the remnant is a short-lived hypermassive NS (Metzger & Fernández 2014; Metzger et al. 2018). Therefore, as the first impression, the low opacity of $\kappa \sim 0.3\ \mathrm{cm^2\ g^{-1}}$ for the peak emission of AT2017gfo seems reasonable, if the remnant NS can live for a short time. However, we would like to point out that the opacity can actually be increased significantly due to the Doppler broadening of bound–bound transitions (Karp et al. 1977), if the material has a very high-velocity gradient, which is indeed the situation in a merger ejecta. Specifically, the Doppler effect due to the velocity gradient can force the photons, with energies that do not strictly match the energy-level differences, to be absorbed, which is forbidden in the laboratory. Therefore, this so-called expansion opacity is dependent on the distributions of density, temperature, and velocity gradient of the ejecta. For a homogenous explosion, the velocity gradient depends on the maximum velocity of the ejecta. In a SN Ia ejecta with a velocity that is about several thousands of $\mathrm{km\ s^{-1}}$, its typical opacity is on the order of $0.1\ \mathrm{cm^2\ g^{-1}}$ for Fe-peak elements (Pinto & Eastman 2000). In contrast, an NS–NS merger typically launches with much greater velocities, reaching a significant fraction of the speed of light. The opacity of such merger ejecta can easily reach $1\ \mathrm{cm^2\ g^{-1}}$, even if only the contributions from open d-shell elements (i.e., Fe, Co, Ni, Ru, et al.) are considered and the effects of lanthanides are ignored (Kasen et al. 2013; Tanaka et al. 2018). In other words, the value of $\sim 1\ \mathrm{cm^2\ g^{-1}}$ gives a conservative lower limit of the opacity of the merger ejecta, which has been widely adopted for lanthanide-free ejecta in the studies before the detection of AT2017gfo (see reviews by Fernández & Metzger 2016; Metzger 2017). As a result, we believe that the low opacity of $\kappa \sim 0.3\ \mathrm{cm^2\ g^{-1}}$ required by the radioactivity-powered mergernova model poses a great challenge to the radioactivity-powered mergernova (or kilonova) model.

Making things worse, for $Y_{\rm e} > 0.25$ that corresponds a low opacity, not only is the lanthanides synthesis blocked, but the synthesis of other heavy elements could also be suppressed significantly. In other words, the radioactive heating rate decreases with an increasing electron fraction (Grossman et al. 2014; Wanajo et al. 2014; Lippuner & Roberts 2015). Specifically, the heating rate as presented in Equation (2) may be relevant for $Y_{\rm e} \sim (0.1$–$0.3)$ but would start to decrease as the electron fraction becomes larger than ~ 0.3. For a relatively high $Y_{\rm e} \sim (0.4$–$0.5)$ that is favored by a low opacity, the heating rate could be reduced by one order of magnitude. This further raises the required ejecta mass (e.g., $\sim 0.4\,M_\odot$) to the unacceptable range.

In summary, the radioactivity-powered mergernova model faces a great challenge, if it is not completely ruled out. As a possible solution to these difficulties, an extra heating source is needed. Such a heating power cannot be provided by the radioactive decay of heavy elements, but can be provided by an underlying engine.

3. Engine-powered Mergernova Model

The chirp mass of the progenitor binary of GW170817 was derived to $M_{\rm c} = 1.188^{+0.004}_{-0.002}\,M_\odot$ from LIGO observations. This constrains the individual masses of the component NSs to be in the range of 1.17–$1.6\,M_\odot$ by assuming low spins for the NSs and the total gravitational mass of the binary to be about $2.74\,M_\odot$ (Abbott et al. 2017a). After the GW chirp and mass ejection, the gravitational mass of the remnant object could be around $M_{\rm RNS} \sim 2.6\,M_\odot$ (Ai et al. 2018; Banik & Bandyopadhyay 2017). The nature of this remnant is subject to debate because of the uncertainties of an NS equation of state. Let us denote the maximum mass of a non-rotating NS by $M_{\rm TOV}$ and the maximum NS mass of a maximally rotating NS as $M_{\rm max}$. The remnant would collapse into a BH promptly, or after a brief hypermassive NS phase, if $M_{\rm max} < M_{\rm RNS}$. For $M_{\rm TOV} < M_{\rm RNS} < M_{\rm max}$, the NS is supramassive and can survive for an extended period of time until centrifugal support can no longer hold against gravity. If $M_{\rm TOV} > M_{\rm RNS}$, then the NS can live permanently. Depending on the outcome of the remnant, the central engine can give rise to different properties of energy injection to power the mergernova.

In the following, we discuss two types of central engines within the framework of the engine-driven mergernova model (Yu et al. 2013, see Appendix).

3.1. BH with Fallback Accretion

We first consider the case that the merger product of GW170817 is a BH (including a prompt BH or a BH formed after a brief hypermassive NS phase). In this case, energy injection from the remnant BH could only be due to fallback accretion. Although most of the ejecta would be unbound, there is still a fraction of mass that is gravitationally bound and would fallback onto the BH during a range of timescales (Rosswog 2007). Initially, the fallback accretion rate keeps constant over a small period of time ~ 0.1 s, and then decays following a power law $\propto t^{-5/3}$. The heating rate to a

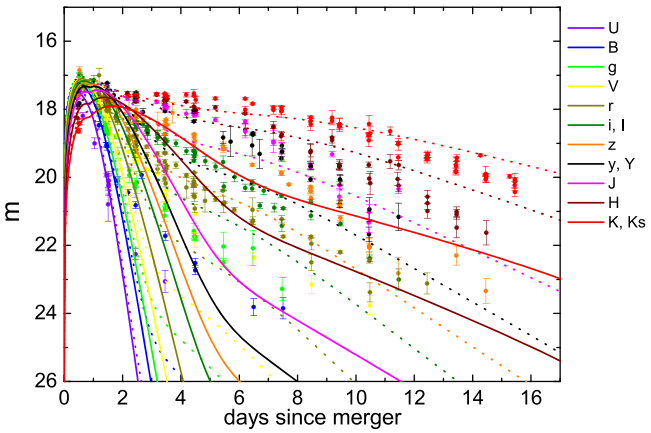

Figure 2. Fitting to the multiband light curves of AT2017gfo with the BH fallback accretion engine. The fitting parameters are shown in Table 1. The solid curves are for central engine-powered emission only. The dotted curves include the contribution from radioactive decay. The data are taken from Villar et al. (2017). The distance is adopted as $D = 40$ Mpc.

mergernova due to this accretion may be calculated by assuming that it is proportional to the accretion rate. We then have (Metzger 2017)

$$L_{\rm fb} = \eta_{\rm fb}\dot{M}_{\rm fb}c^2 \tag{5}$$

$$\approx 2 \times 10^{51}\,{\rm erg\ s^{-1}}\left(\frac{\eta_{\rm fb}}{0.1}\right)\left(\frac{\dot{M}_{\rm fb,i}}{10^{-3}\,M_\odot\ {\rm s^{-1}}}\right)\left(\frac{t}{0.1\ {\rm s}}\right)^{-5/3}, \tag{6}$$

where $\dot{M}_{\rm fb}$ is the accretion rate with the subscript "i" standing for "initial", and $\eta_{\rm fb}$ represents the fraction of the accretion energy that can be ejected outwards (i.e., accretion feedback efficiency).

Tentative fitting with such an accretion-induced heating rate to the multiband light curves of AT2017gfo is presented in Figure 2. Without a radioactive power included (solid curves), the model can only account for the early blue component. In this fitting, the opacity is fixed to $\kappa = 1\,{\rm cm^2\,g^{-1}}$ for the polar blue ejecta and $\kappa = 5\,{\rm cm^2\,g^{-1}}$ for the equatorial ejecta, corresponding to the lanthanide-free and lanthanide-rich ejecta, respectively. The values of the other parameters are taken freely and their values are presented in Table 1. For the adopted feedback efficiency of $\eta_{\rm fb} = 0.1$ (Metzger 2017), the initial accretion rate is required to be $\dot{M}_{\rm fb,i} = 3 \times 10^{-3}\,\dot{M}_\odot\ {\rm s^{-1}}$, which corresponds to a total mass of $7.5 \times 10^{-4}\,M_\odot$ of the fallback material. In principle, the feedback efficiency $\eta_{\rm fb}$ can be (much) smaller than 0.1, which would lead to a requirement of a much higher and even unacceptable fallback accretion rate. In any case, because the accretion heating decays very quickly ($\propto t^{-5/3}$), the late-time emission of AT2017gfo always needs to be powered by radioactive decay so that the required ejecta mass is still substantial (e.g., $\sim 0.05\,M_\odot$; Villar et al. 2017). According to numerical simulations, such a high ejecta mass is only available for BH-NS mergers (Foucart et al. 2013), but not for an NS–NS merger like GW170817. We therefore conclude that energy injection due to BH fallback accretion cannot satisfactorily interpret the data.

3.2. Spinning-down NS

The difficulty of the fallback accretion model suggests that the central engine of AT2017gfo should be long lasting, at least for more than 10 days. The merger product can only be a supramassive or even a permanently stable NS. Such an NS has long been suggested as the central engine of GRBs (Dai & Lu 1998a, 1998b; Zhang & Mészáros 2001; Dai et al. 2006), superluminous supernovae (Kasen & Bildsten 2010; Woosley 2010), and also mergernovae (Yu et al. 2013; Metzger & Piro 2014; Yu et al. 2018). Different from Yu et al. (2018), who invoked an NS to interpret the late-time emission of AT2017gfo, this Letter invokes the NS power to interpret the entire (blue and red) emission of AT2017gfo.

As analyzed by Yu et al. (2018), the surface dipolar magnetic filed of the remnant NS of GW170817 cannot be very high if the NS spins at a near-Keplerian frequency initially, because of the constraints posed by the mergernova luminosity and timescale. A similar constraint can be also derived from the multi-wavelength data (Ai et al. 2018). In order to spin down the NS significantly, efficient secular GW spindown is needed. In the GW-spindown-dominated regime, the temporal evolution of the luminosity of the magnetic dipole radiation of the NS, which is absorbed by the merger ejecta, can be expressed as

$$L_{\rm md} = L_{\rm md,i}\left(1 + \frac{t}{t_{\rm sd,gw}}\right)^{-1} \tag{7}$$

with

$$L_{\rm md,i} = 9.6 \times 10^{42}\,{\rm erg\ s^{-1}}\,R_6^6 B_{12}^2 P_{\rm i,-3}^{-4} \tag{8}$$

and

$$t_{\rm sd,gw} = 9.1 \times 10^3\ {\rm s}\ \epsilon_{-3}^{-2} I_{45}^{-1} P_{\rm i,-3}^4 \tag{9}$$

where R, B, Pi, and I are the radius, surface magnetic field, initial spin period, and the moment of inertia of the NS, respectively. The conventional notation $Q_x = Q/10^x$ is adopted in cgs units.

A model fit to the multi-wavelength light curves of AT2017gfo with energy injection of a low-B NS is presented in Figure 3, which shows that both the early and late emission of AT2017gfo can well be accounted for by this model. The model parameters are collected in Table 1. In this model, one also needs two ejecta components. The masses of the polar and equatorial ejecta are both required to be on the order of $10^{-3}\,M_\odot$, which comfortably match the values of NS–NS merger simulations. The heating due to radioactive decay is no longer important during the entire emission episode, and the mergernova is dominantly powered by energy injection from the NS. The GW-dominated spindown timescale is adopted as $t_{\rm sd,g} = 500\,{\rm s}$, which is inspired by the extended emission or plateaus in SGRBs (Rowlinson et al. 2013; Lü et al. 2015). The initial magnetic dipole luminosity can be then constrained to be $L_{\rm md,i} = 3.4 \times 10^{44}\,{\rm erg\ s^{-1}}$. For an initial Keplerian spin period $P_{\rm i} = 1$ ms, the ellipticity and the surface dipolar magnetic field of the NS can be derived as

$$\epsilon = 0.0035 \tag{10}$$

and

$$B = 3.4 \times 10^{12}\,{\rm G}, \tag{11}$$

Table 1
Fitting Parameters

	$M_{\rm fb,i}/M_\odot\ {\rm s}^{-1}$	$L_{\rm md,i}/{\rm erg\ s}^{-1}$	$t_{\rm sd,gw}/{\rm s}$	B/G	ϵ	Ejecta	$M_{\rm ej}/M_\odot$	$\kappa/{\rm cm}^2\ {\rm g}^{-1}$	$v_{\rm ej,i}/c$	Ω	δ	ζ	A
Fallback	3×10^{-3}	...	...	...	...	Polar	3×10^{-3}	1	0.25	2π	-1	10	6
						Equatorial	5×10^{-2}	5	0.15	2π	-1	10	6
NS	...	3.4×10^{44}	500	3.4×10^{12}	0.0035	Polar	1×10^{-3}	1	0.35	2π	-1	10	6
						Equatorial	5×10^{-3}	5	0.2	2π	-1	10	6

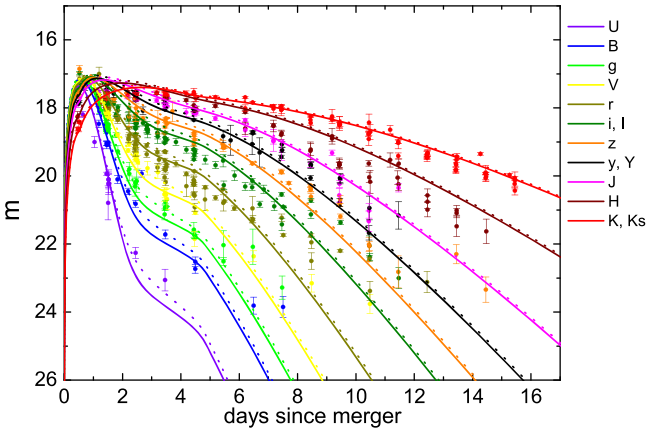

Figure 3. Same as in Figure 2 but for energy injection from a spinning-down NS. The fitting parameters are also shown in Table 1. With small ejecta masses for both the polar and equatorial components, heating due to radioactive decay is no longer important for powering the observed emission during the entire duration of the event.

where a stellar radius of $R = 1.2\times10^6$ cm and a moment of inertia of $I = 1.5\times10^{45}\ {\rm g\ cm}^2$ are adopted. According to these parameters, the remnant NS during the mergernova timescale should have a very high deformation but a relatively normal poloidal surface magnetic field. These results are consistent with the constraints recently given by Ai et al. (2018) and Yu et al. (2018), and is also consistent with the requirement of interpreting internal X-ray plateaus in short GRBs (Fan et al. 2013; Gao et al. 2016). Specifically, the surface magnetic field found here is about an order of magnitude higher than that found by Yu et al. (2018), i.e., $\sim10^{12}$ G versus $\sim10^{11}$ G. This relatively normal strength of the dipolar magnetic field could be just an effective strength corresponding to the required spin-down luminosity. The high ellipticity of the remnant NS strongly suggests that its internal (probably toroidal) magnetic fields are ultrahigh, i.e., the NS is a magnetar. Then, the surface magnetic field of the NS could also be intrinsically much higher than $\sim10^{12}$ G, which could however be significantly buried and/or exist in the form of a multipolar filed (see Yu et al. 2018 for a detailed discussion). In any case, the existence of a long-lived NS is also helpful to interpret the broadband afterglow of the event (Geng et al. 2018).

4. Summary and Conclusions

Based on the traditional radioactivity-powered mergernova (kilonova) model, we used the peak bolometric luminosity and peak emission time of AT2017gfo to estimate the parameters of the merger ejecta and obtained a large ejecta mass $\sim0.04\,M_\odot$ and a low opacity of $\kappa\sim0.3\ {\rm cm}^2\ {\rm g}^{-1}$. These are broadly consistent with more detailed modeling by many authors. On the other hand, we argue that this set of parameters is difficult to achieve within the framework of NS–NS mergers without a long-lasting central engine. In particular, the required κ is too low even for lanthanide-free ejecta. Even though a high $Y_{\rm e}$ is achieved, it is hard to reduce κ to the desired value. Furthermore, radioactive heating becomes inefficient with a high $Y_{\rm e}$, so that an even larger ejecta mass is needed to achieve the desired peak flux. These pose a problem for the standard model.

We then argue that a simple fix for this problem is to introduce a central engine that can provide continuous energy injection to power the mergernova emission. We find that a BH with fallback accretion may power the bright early blue emission component of AT2017gfo, but the late red component still needs radioactive heating of a massive ejecta inconsistent with the numerical results of NS–NS mergers. This only leaves us the option of having a long-lived, low-B NS as the central engine. We show that the multiband light curves of AT2017gfo can well be reproduced by such an engine-driven mergernova model, where both the opacity κ and the ejected mass values for both the blue and red components fall into the reasonable ranges of known numerical simulations. This enhances the suggestion (Yu et al. 2018) of a long-lived NS as the merger remnant of GW170817 (see also Ai et al. 2018; Geng et al. 2018).

In addition to the engine-powered mergernova model discussed here, we would also like to mention that Piro & Kollmeier (2018) suggested that the blue emission component of AT2017gfo can be explained by the cooling of a shocked cocoon. The cocoon energy is generated by the shock interaction between a relativistic GRB jet and the surrounding envelope. In principle, this shock interaction may be also regarded as a kind of energy injection. Furthermore, Matsumoto et al. (2018) suggested that both the blue and red emission components could be powered by energy injections from a jet and X-rays, respectively (see Kisaka et al. 2016 for the original suggestion of X-ray powered macronova, which is the kilonova and mergernova discussed in this Letter). Murase et al. (2018) discussed the possibility of differentiating the BH versus NS engine using high-energy emission from NS–NS merger systems.

This work is supported by the National Basic Research Program of China (973 Program, grant 2014CB845800), the National Natural Science Foundation of China (grant No. 11473008 and 11573014), and the Self-Determined Research Funds of CCNU from the colleges' basic research and operation of MOE. S.-Z. Li and L.-D. Liu are supported by scholarships from the China Scholarship Council (No. 201706770050 and No. 201706190127) to conduct research at the University of Nevada, Las Vegas (UNLV).

Appendix
The Model

Because the merger ejecta turns out to be mild relativistic, we reduce the mergernova model (Yu et al. 2013) into the Newtonian form. This semi-analytical model is also developed by involving the density profile of the ejecta in order to give a better description about the multiband light curves. Numerical simulations suggest that the density profile of the dynamical ejecta cannot be fitted with only one single power law (Piran et al. 2013). In addition, a central engine may significantly modify the density profile into a shell-like structure (Kasen et al. 2016). Here we generally adopt a broken power-law profile

$$\rho(r) = \rho_0\left(\frac{r}{R_{\rm ej}}\right)^{-\delta}, \qquad r \leqslant R_{\rm ej}, \tag{12a}$$

$$\rho(r) = \rho_0\left(\frac{r}{R_{\rm ej}}\right)^{-\zeta}, \qquad r > R_{\rm ej}, \tag{12b}$$

where $R_{\rm ej}$ is the radius of the main ejecta, $\rho_0 = (3-\delta)(\zeta-3)M_{\rm ej}/4\pi(\zeta-\delta)R_{\rm ej}^3$ is the density at $R_{\rm ej}$, and $M_{\rm ej}$ is the mass. This is very similar to the density profile of a supernova (Kasen et al. 2016). The difference here is that the parameter δ is adopted as a negative value to represent a shell-like structure. The density profile is expected to be shallow in the inner ejecta, $r \leqslant R_{\rm ej}$, but become very steep in the outer ejecta, $r > R_{\rm ej}$. So the parameter ζ is adopted as a relatively large positive value. This profile avoids the infinite integral mass problem, so that a sudden cut-off is not introduced.

The basic energy conservation equation is

$$\frac{dE}{dt} = -P\frac{dV}{dt} - L_{\rm e} + L_{\rm in}, \tag{13}$$

where E is internal energy, $L_{\rm e}$ is emission luminosity, $L_{\rm in}$ is energy injection rate, $V = 4\pi R_{\rm ej}^3/3$ is the main volume, and

$$P = \frac{E}{3V} - \frac{L_{\rm e}}{4\pi R_{\rm ej}^2 c} \tag{14}$$

is the effective (radiation dominated) pressure (with the second term in Equation (14) taking care of the leakage of radiation pressure), and PdV represents the energy lose due to adiabatic expansion. Since the density out of $R_{\rm ej}$ drops fast due to large ζ, the velocity of ejecta is defined as $v_{\rm ej} = dR_{\rm ej}/dt$. The initial velocity $v_{\rm ej,i}$ is treated as a free parameter. Due to continuous energy injection, the ejecta would be accelerated with

$$\frac{dv_{\rm ej}}{dt} = \frac{4\pi R_{\rm ej}^2 P}{M_{\rm ej}}. \tag{15}$$

Our treatment includes both central engine heating and radioactive heating. The difference is that the former has the heating source at the bottom, while the latter has heating throughout the ejecta. This result is a small difference in calculating the optical depth of the ejecta, with

$$\tau = \frac{(\zeta-\delta)\kappa\rho_0 R_{\rm ej}}{(1-\delta)(\zeta-1)} \tag{16}$$

denoting the integral optical depth from the bottom, which is relevant for central engine heating, and

$$\tilde{\tau} \simeq \tau/\beta \tag{17}$$

is relevant for radioactive heating, where $\beta \sim 3$ is a dimensionless parameter reflecting the averaging effect in the ejecta (Arnett 1982; Metzger et al. 2010).

The emission luminosities for the central engine (subscript "c") and radioactive (subscript "r") components can be written as (Kasen & Bildsten 2010; Yu et al. 2013)

$$L_{\rm e,c} = \frac{E_{\rm c}c}{\tau R_{\rm ej}}, \qquad \text{for } \tau \geqslant 1, \tag{18a}$$

$$L_{\rm e,c} = \frac{E_{\rm c}c}{R_{\rm ej}}, \qquad \text{for } \tau < 1, \tag{18b}$$

$$L_{\rm e,r} = \frac{E_{\rm r}c}{\tilde{\tau} R_{\rm ej}}, \qquad \text{for } \tilde{\tau} \geqslant 1, \tag{19a}$$

$$L_{\rm e,r} = \frac{E_{\rm r}c}{R_{\rm ej}}, \qquad \text{for } \tilde{\tau} < 1, \tag{19b}$$

where c is the speed of light, and the total internal energy is $E = E_{\rm c} + E_{\rm r}$.

For a central engine, the bolometric light curve would peak at the photon diffusion timescale (Kasen & Bildsten 2010; Yu et al. 2015), i.e.,

$$t_{\rm d} \approx (3\kappa M_{\rm ej}/4\pi v_{\rm ej} c)^{1/2}, \tag{20}$$

if the density is uniform ($\delta = 0$). When the density profile is fully considered, this gives

$$t_{\rm d} \approx \left[\frac{(3-\delta)(\zeta-3)\kappa M_{\rm ej}}{(1-\delta)(\zeta-1)4\pi v_{\rm ej} c}\right]^{1/2}, \tag{21}$$

which depends on the parameters δ and ζ.

The spectrum of emission is a blackbody when $\tau \geqslant 1$ but would be somewhat deviated when $\tau < 1$. Near the peak, the ejecta is still optically thick. One can define the effective temperature $T_{\rm eff} = \sqrt[4]{L_{\rm e}/4\pi R_{\rm ph}^2\sigma}$, where $R_{\rm ph}$ is the photosphere radius at which the optical depth from $R_{\rm ph}$ to the outer edge of ejecta drops to unity.[8] In our calculation, the spectrum is assumed to be a blackbody all of the time. This is valid before and slightly after the peak, but would not be valid at later times. When the ejecta becomes optically thin, a modified photosphere radius $R'_{\rm ph} = R_{\rm ej} - (V_{\rm ej} - V_{\rm ph})/4\pi R_{\rm ej}^2$ instead of $R_{\rm ph}$ is used to calculate effective temperature. The observed flux can be then given by

$$F_\nu = \frac{2\pi h\nu^3}{c^2}\frac{1}{\exp[h\nu/k_{\rm B}T_{\rm eff}] - 1}\left(\frac{R_{\rm ph}}{D}\right)^2, \tag{22}$$

where ν is frequency, D is distance, and h and $k_{\rm B}$ are the Plank constant and Boltzmann constant, respectively.

The injected energy from the central engine would not be fully deposited into ejecta. For simplicity, an efficiency of $\eta_0 = 0.5$ is adopted for both central engine heating and radioactive heating. When the ejecta becomes optically thin, the efficiency of central engine heating would be related to the

[8] Notice that once a velocity is derived from a spectrum analysis, the velocity should be the photosphere velocity that is determined by $v_{\rm ph} = v_{\rm ej}R_{\rm ph}/R_{\rm ej}$.

optical depth, i.e.,

$$\eta_{\rm c} = \eta_0(1 - e^{-A\tau}), \quad (23)$$

where the parameter A represents a characteristic efficiency decay rate. Similarly, the efficiency corresponding to radioactive heating is given by

$$\eta_{\rm r} = \eta_0(1 - e^{-A\tilde{\tau}}). \quad (24)$$

The total energy injection from both central engine and radioactive heating can be expressed as

$$L_{\rm in} = L_{\rm c} + L_{\rm r} = \eta_{\rm c} L_{\rm c} + \eta_{\rm r}\varepsilon M_{\rm ej}, \quad (25)$$

where $L_{\rm c}$ is the central engine and ε is the heating rate from radioactive decay. So, once $L_{\rm c}$ and ε are given, the differential equations can be solved.

When two heating sources are invoked, separate differential equations analogous to Equations (13)–(15) for both the central engine heating and radioactive heating are solved.

In the above treatment, an isotropic ejecta (with solid angle 4π) is assumed. When fitting the data of AT2017gfo, we have divided the ejecta into two components, a blue polar component with solid angle $\Omega_{\rm p}$ and a red equatorial component with solid angle $\Omega_{\rm e}$. In our model fitting, both components have a solid angle 2π, and the relevant ejecta parameters (κ and M) are fitted separately (see Table 1).

ORCID iDs

Shao-Ze Li https://orcid.org/0000-0002-9866-2795
Yun-Wei Yu https://orcid.org/0000-0002-1067-1911
Bing Zhang https://orcid.org/0000-0002-9725-2524

References

Abbott, B. P., Abbott, R., Abbott, T. D., et al. 2016, PhRvL, 116, 061102
Abbott, B. P., Abbott, R., Abbott, T. D., et al. 2017a, PhRvL, 119, 161101
Abbott, B. P., Abbott, R., Abbott, T. D., et al. 2017b, ApJL, 848, L13
Ai, S., Gao, H., Dai, Z.-G., et al. 2018, ApJ, 860, 57
Arcavi, I., Hosseinzadeh, G., Howell, D. A., et al. 2017, Natur, 551, 64
Arnett, W. D. 1982, ApJ, 253, 785
Banik, S., & Bandyopadhyay, D. 2017, arXiv:1712.09760
Barnes, J., & Kasen, D. 2013, ApJ, 775, 18
Barnes, J., Kasen, D., Wu, M.-R., & Martínez-Pinedo, G. 2016, ApJ, 829, 110
Bauswein, A., Goriely, S., & Janka, H.-T. 2013, ApJ, 773, 78
Coulter, D. A., Foley, R. J., Kilpatrick, C. D., et al. 2017, Sci, 358, 1556
Cowperthwaite, P. S., Berger, E., Villar, V. A., et al. 2017, ApJL, 848, L17
Dai, Z. G., & Lu, T. 1998a, A&A, 333, L87
Dai, Z. G., & Lu, T. 1998b, PhRvL, 81, 4301
Dai, Z. G., Wang, X.-Y., Wu, X.-F., & Zhang, B. 2006, Sci, 311, 1127
Dessart, L., Ott, C. D., Burrows, A., Rosswog, S., & Livne, E. 2009, ApJ, 690, 1681
Fan, Y.-Z., Wu, X.-F., & Wei, D.-M. 2013, PhRvD, 88, 067304
Fernández, R., Kasen, D., Metzger, B. D., & Quataert, E. 2015, MNRAS, 446, 750
Fernández, R., & Metzger, B. D. 2013, MNRAS, 435, 502
Fernández, R., & Metzger, B. D. 2016, ARNPS, 66, 23
Foucart, F., Deaton, M. B., Duez, M. D., et al. 2013, PhRvD, 87, 084006
Gao, H., Zhang, B., & Lü, H.-J. 2016, PhRvD, 93, 044065
Geng, J.-J., Dai, Z.-G., Huang, Y.-F., et al. 2018, ApJL, 856, L33
Goldstein, A., Veres, P., Burns, E., et al. 2017, ApJL, 848, L14
Grossman, D., Korobkin, O., Rosswog, S., & Piran, T. 2014, MNRAS, 439, 757
Hotokezaka, K., Kiuchi, K., Kyutoku, K., et al. 2013, PhRvD, 87, 024001
Just, O., Bauswein, A., Ardevol Pulpillo, R., Goriely, S., & Janka, H.-T. 2015, MNRAS, 448, 541
Karp, A. H., Lasher, G., Chan, K. L., & Salpeter, E. E. 1977, ApJ, 214, 161
Kasen, D., Badnell, N. R., & Barnes, J. 2013, ApJ, 774, 25
Kasen, D., & Bildsten, L. 2010, ApJ, 717, 245
Kasen, D., Fernández, R., & Metzger, B. D. 2015, MNRAS, 450, 1777
Kasen, D., Metzger, B., Barnes, J., Quataert, E., & Ramirez-Ruiz, E. 2017, Natur, 551, 80
Kasen, D., Metzger, B. D., & Bildsten, L. 2016, ApJ, 821, 36
Kisaka, S., Ioka, K., & Nakar, E. 2016, ApJ, 818, 104
Korobkin, O., Rosswog, S., Arcones, A., & Winteler, C. 2012, MNRAS, 426, 1940
Li, L.-X., & Paczyński, B. 1998, ApJL, 507, L59
Li, S.-Z., & Yu, Y.-W. 2016, ApJ, 819, 120
Lippuner, J., & Roberts, L. F. 2015, ApJ, 815, 82
Lipunov, V. M., Kornilov, V., Gorbovskoy, E., et al. 2017, MNRAS, 465, 3656
Lü, H.-J., Zhang, B., Lei, W.-H., Li, Y., & Lasky, P. D. 2015, ApJ, 805, 89
Ma, S.-B., Lei, W.-H., Gao, H., et al. 2018, ApJL, 852, L5
Matsumoto, T., Ioka, K., Kisaka, S., & Nakar, E. 2018, arXiv:1802.07732
Metzger, B. D. 2017, LRR, 20, 3
Metzger, B. D., & Fernández, R. 2014, MNRAS, 441, 3444
Metzger, B. D., Martínez-Pinedo, G., Darbha, S., et al. 2010, MNRAS, 406, 2650
Metzger, B. D., & Piro, A. L. 2014, MNRAS, 439, 3916
Metzger, B. D., Thompson, T. A., & Quataert, E. 2018, ApJ, 856, 101
Murase, K., Toomey, M. W., Fang, K., et al. 2018, ApJ, 854, 60
Nicholl, M., Berger, E., Kasen, D., et al. 2017, ApJL, 848, L18
Perego, A., Rosswog, S., Cabezón, R. M., et al. 2014, MNRAS, 443, 3134
Pinto, P. A., & Eastman, R. G. 2000, ApJ, 530, 757
Piran, T., Nakar, E., & Rosswog, S. 2013, MNRAS, 430, 2121
Piro, A. L., & Kollmeier, J. A. 2018, ApJ, 855, 103
Radice, D., Perego, A., Bernuzzi, S., & Zhang, B. 2018, arXiv:1803.10865
Richers, S., Kasen, D., O'Connor, E., Fernández, R., & Ott, C. D. 2015, ApJ, 813, 38
Rosswog, S. 2007, MNRAS, 376, L48
Rosswog, S. 2013, RSPTA, 371, 20120272
Rosswog, S., Feindt, U., Korobkin, O., et al. 2017, CQGra, 34, 104001
Rowlinson, A., O'Brien, P. T., Metzger, B. D., Tanvir, N. R., & Levan, A. J. 2013, MNRAS, 430, 1061
Savchenko, V., Ferrigno, C., Kuulkers, E., et al. 2017, ApJL, 848, L15
Shibata, M., Kiuchi, K., & Sekiguchi, Y.-i. 2017, PhRvD, 95, 083005
Siegel, D. M., & Metzger, B. D. 2018, ApJ, 858, 52
Smartt, S. J., Chen, T.-W., Jerkstrand, A., et al. 2017, Natur, 551, 75
Song, C.-Y., Liu, T., & Li, A. 2018, MNRAS, 477, 2173
Tanaka, M., & Hotokezaka, K. 2013, ApJ, 775, 113
Tanaka, M., Kato, D., Gaigalas, G., et al. 2018, ApJ, 852, 109
Tanaka, M., Utsumi, Y., Mazzali, P. A., et al. 2017, PASJ, 69, 102
Tanvir, N. R., Levan, A. J., González-Fernández, C., et al. 2017, ApJL, 848, L27
Troja, E., Piro, L., van Eerten, H., et al. 2017, Natur, 551, 71
Valenti, S., David, Sand, J., et al. 2017, ApJL, 848, L24
Villar, V. A., Guillochon, J., Berger, E., et al. 2017, ApJL, 851, L21
Wanajo, S., Sekiguchi, Y., Nishimura, N., et al. 2014, ApJL, 789, L39
Waxman, E., Ofek, E., Kushnir, D., & Gal-Yam, A. 2017, arXiv:1711.09638
Woosley, S. E. 2010, ApJL, 719, L204
Yu, Y.-W., Li, S.-Z., & Dai, Z.-G. 2015, ApJL, 806, L6
Yu, Y.-W., Liu, L.-D., & Dai, Z.-G. 2018, ApJ, in press (arXiv:1711.01898)
Yu, Y.-W., Zhang, B., & Gao, H. 2013, ApJL, 776, L40
Zhang, B., & Mészáros, P. 2001, ApJL, 552, L35
Zhang, B.-B., Zhang, B., Sun, H., et al. 2018, NatCo, 9, 447